Acta Cryst. (1975). A31, 300

n-Beam Lattice Images. V. The Use of the Charge-Density Approximation in the Interpretation of Lattice Images

BY D. F. LYNCH AND A. F. MOODIE
Division of Chemical Physics, CSIRO, P.O. Box 160, *Clayton, Victoria, Australia* 3168

AND M. A. O'KEEFE
Division of Tribophysics, CSIRO, University of Melbourne, Parkville, Victoria, Australia 3052

(*Received* 5 *November* 1974; *accepted* 26 *December* 1974)

The simple infinite-aperture charge-density approximation to lattice imaging is extended to include the effects of finite aperture and objective-lens spherical aberration. Images computed using these approximations are compared with images computed by the accurate *N*-beam technique and with experiment in order to establish the bounds of applicability of the extended-charge-density approximations.

1. Introduction

It is clear that for many electron micrographs an intuitive interpretation of the contrast is possible in terms of an amplitude object. A brief account of the charge-density approximations has been given in the earlier papers of this series (Allpress, Hewat, Moodie & Sanders, 1972; Lynch & O'Keefe, 1972; Anstis, Lynch, Moodie & O'Keefe, 1973; O'Keefe, 1973)* and these approximations explain why such intuitive interpretations are valid. It is appropriate, then, to give a more detailed description of the approximations, to investigate their bounds, and the level to which they agree with experiment. The application of these methods to non-periodic objects is treated elsewhere (Lynch, Moodie & O'Keefe, 1974).

2. Theory

The contrast of an image formed in the electron microscope is calculated by first determining the complex amplitudes of the waves scattered by the object. These waves are then combined with suitable aberration parameters, multiplied by the propagation function appropriate to the defect of focus from the Gaussian image plane, multiplied by the aperture function, and Fourier transformed to obtain the image amplitudes; the latter are then squared to obtain the contrast. As has been shown in the preceding papers of this series, the first step of the calculation is the most time-consuming. In the series *n* is used to denote the number of diffracted beams summed to obtain image contrast and *N* is used to denote the number of reflexions used in the dynamic scattering calculation.

* This series of publications on *n*-beam lattice images was commenced at a time when it appeared that *Acta Crystallographica* was about to adopt nm as a standard of length, thus for the sake of consistency we have retained nm as a unit rather than the more usual Å.

2.1. *Scattering approximations*

For high voltages the correct limiting form of the *N*-beam solution to the electron scattering as the accelerating voltage tends to infinity is given by

$$U_{HVL}(u,v)=\mathscr{F}[\exp\{i\sigma_c\int_0^H\varphi(x,y,z)\mathrm{d}z\}], \qquad (1)$$

where σ_c is the Compton interaction parameter, H is the crystal thickness, φ is the crystal potential and $\mathscr{F}$ signifies the Fourier transform (Moodie, 1972). At infinite voltage this solution accurately takes into account the dynamical interactions within the crystal, and so applies to crystals of any thickness. At lower voltages, if σ_c is replaced by $\sigma\{\sigma=(\pi/\lambda W)\,(2/[1+(1-\beta^2)^{1/2}]);$ $W=$ accelerating voltage, $\lambda=$ wavelength, $\beta=v/c\}$, it is a good approximation up to some thickness which depends upon the voltage. For example, when the accelerating voltage is 100 kV it gives a good approximation to the waves scattered by a crystal composed of medium-weight atoms and oriented with the incident beam nearly parallel to a principal axis, provided that the thickness is less than about 5 nm.

As the crystal thickness H tends to zero, or the projected potential $\varphi_p(x,y)=\int_0^H\varphi(x,y,z)\mathrm{d}z$ tends to zero, the high-voltage limit tends to

$$U_B(u,v)=\mathscr{F}\{1+i\sigma\varphi_p(x,y)\}. \qquad (2)$$

This is the form for the scattered wave used by Scherzer (1949) and recently used extensively for the estimation of image contrast. However, the amplitudes and phases for some important reflexions, calculated from equation (2), depart significantly from the *N*-beam solutions for a crystal of $Nb_{12}O_{29}$ only 1 nm thick, whereas those calculated from the high-voltage limit using equation (1) remain in fair agreement to about 5 nm (Fig. 1). In general the errors in the Scherzer approximation will lead to serious errors in the estimation of image contrast for crystals greater than 1 nm in thickness.

Moreover the high-voltage limit holds to greater crystal thicknesses and, as can be seen from equations (1) and (2), contains the Scherzer approximation. Within this region of applicability the high-voltage limit can be used to simplify the calculation of lattice-image contrast.

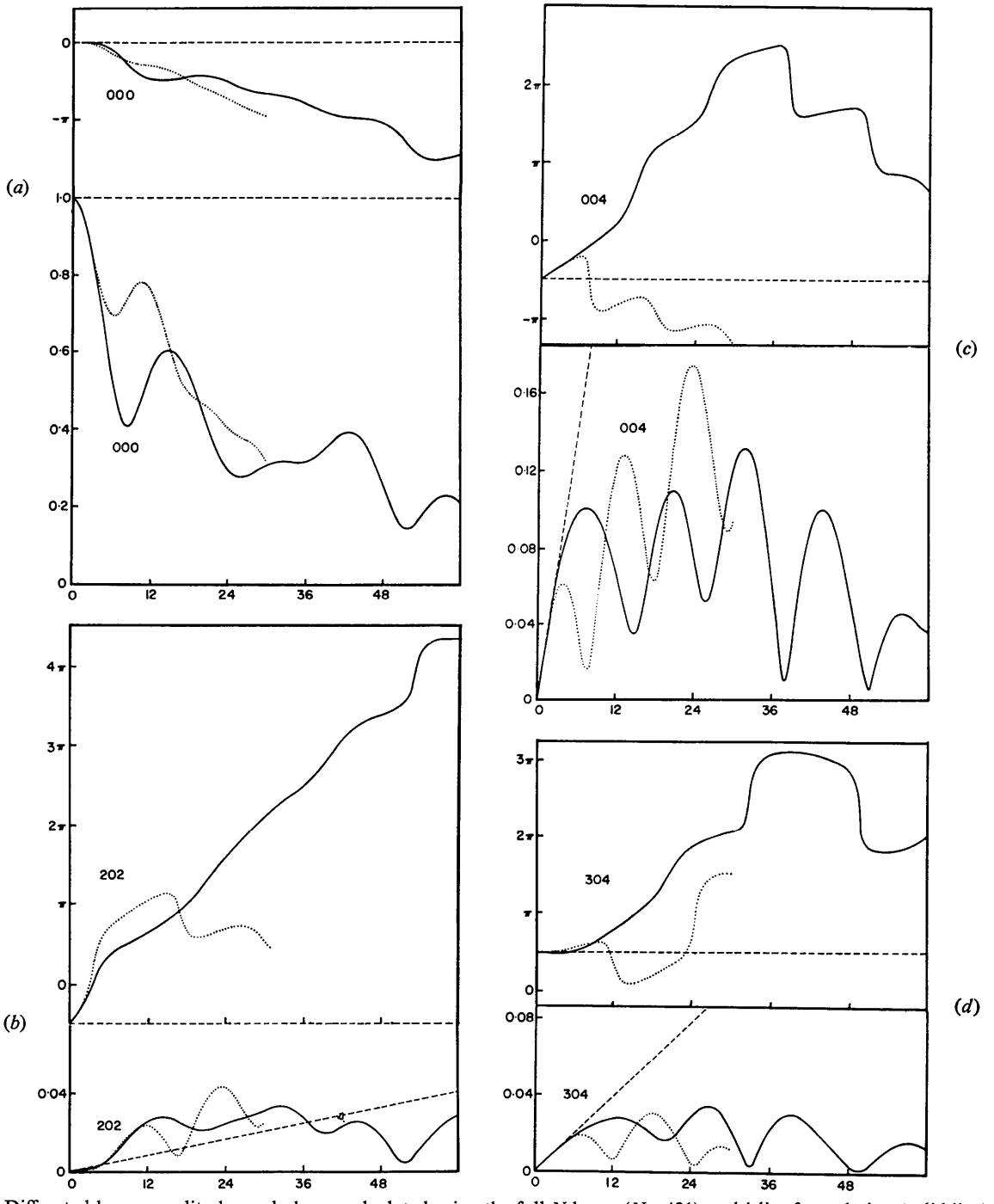

Fig. 1. Diffracted-beam amplitudes and phases calculated using the full N-beam ($N=421$) multislice formulation (solid line), the high-voltage-limit (HVL) approximation (dotted line) and the single-scattering (kinematic) theory (dashed line) for $Nb_{12}O_{29}$ up to 60 nm thick with electrons of 100 keV incident energy. Overall the departure of the kinematic curves from the N-beam curves occurs at lower crystal thicknesses than equivalent departures for the HVL-calculated amplitude and phases. This is immediately obvious for beams like the 000 (*a*), but, even where the kinematic amplitudes are closer to the N-beam values than are the HVL ones, the HVL phases match the N-beam phases to greater thicknesses than do the kinematic phases (*e.g.*, the 202 (*b*) and 004 (*c*)]. For some weak beams both amplitude and phase curves remain close together for all three calculations for thicknesses up to 5 nm (*e.g.*, the 304 (*d*)].

All the preceding arguments have been for the case of a crystal oriented such that the incident beam is nearly parallel to a principal axis, that is, the case of a zone-axis diffraction pattern. If the crystal is tilted so that there is only a line of strong reflexions, a systematics orientation, then the high-voltage limit is valid for a thicker crystal (Goodman & Moodie, 1974).

2.2 *Thin lens – infinite aperture*

The simplest theoretical treatment using the high-voltage limit considers the image formed by a perfect thin lens of infinite aperture (Cowley & Moodie, 1960). The out-of-focus condition is then generated by a propagation function of the form

$$P(h,k)=\exp\{-i\pi\varepsilon\lambda(u^2+v^2)\}, \qquad (3)$$

where ε = the distance (nm) from the Gaussian focus of the lens, negative being underfocus. This propagation function then multiples the wave function and the image contrast is obtained from the square of the modulus of the Fourier transform of the resulting amplitudes and phases. If we follow Cowley & Moodie (1960) and expand the propagation function as

$$P(h,k)=1-i\pi\varepsilon\lambda(u^2+v^2), \qquad (4)$$

then the wave function on the image plane becomes

$$\psi_\varepsilon(x,y)=\mathscr{F}^{-1}[\{\mathscr{F}[\exp(i\sigma\varphi_p)]\}\,.\,\{1-i\pi\varepsilon\lambda(u^2+v^2)\}]$$
$$=\exp(i\sigma\varphi_p)\left[1-\frac{\varepsilon\lambda\sigma}{4\pi}\left\{\nabla^2\varphi_p+i\sigma\left\{\left(\frac{\partial\varphi_p}{\partial x}\right)^2+\left(\frac{\partial\varphi_p}{\partial y}\right)^2\right\}\right\}\right],$$

where $\mathscr{F}$ denotes Fourier transformation, and the image contrast to first order in σ (Moodie, 1975) is

$$I_\varepsilon(x,y)=\psi^*\psi=(C^2+S^2)\left[1-\frac{\varepsilon\sigma\lambda}{2\pi}\nabla^2\varphi_p(x,y)\right], \qquad (5)$$

where $C+iS=\exp(i\sigma\varphi_p)$ represents the Fourier transform of high-voltage-limit amplitudes and phases, and, at infinite aperture, $|C+iS|^2=1$. Hence the only term giving appreciable contrast is that which is proportional to the second differential of the projected potential, that is, the projected charge density of the crystal. This term is multiplied by the defect of focus, ε, so that within the limit that $\varepsilon\lambda(u^2+v^2)<\frac{1}{2}$ (the criterion that the original expansion of the propagator is valid) the contrast is proportional to the defect of focus. The contrast is zero on the Gaussian focus ($\varepsilon=0$) and is complimentary (antisymmetric) between positive and negative defects of focus. Because σ contains the electron charge the under-focus image will have high density corresponding to regions of high projected charge density; the overfocus image will be the reverse.

2.3 *Finite aperture*

A more realistic description requires that the lens be of finite aperture. The high-voltage limit tells us that an object, represented by a potential distribution, can be described in terms of an equivalent phase object. For infinite aperture the intensity distribution of the image of this phase object is equivalent to the charge-density distribution obtained from the second differential of the potential, over a range of defects of focus. The application of the Rayleigh theory of image formation to the equivalent phase object cannot be expected to give the same intensity distributions as the application of that theory to the amplitude object represented by the charge density. But in fact, with appropriately large aperture, the results are sufficiently similar to allow a simple interpretation.

The amplitude distribution on the image plane of the infinite aperture lens, to first order in σ and ε, is

$$\psi(x,y)=q(x,y)\left[1-\frac{\varepsilon\lambda}{4\pi}\sigma\nabla^2\varphi_p\right], \qquad (6)$$

where $q(x,y)=\exp(i\sigma\varphi_p)$. Then, on Fourier transformation of equation (6) and multiplication by an aperture function $A(u,v)=1$ for $(u^2+v^2)^{1/2}<r$, $A(u,v)=0$ for $(u^2+v^2)^{1/2}>r$, we obtain

$$\mathscr{F}\{\psi(x,y)\}\,.\,A=\sum_{hk}Q_{hk}\delta\left(u-\frac{h}{a},v-\frac{k}{b}\right).A$$
$$+4\pi\varepsilon\lambda\sigma\left[\sum_{hk}Q_{hk}\delta\left(u-\frac{h}{a},v-\frac{k}{b}\right)\right.$$
$$\left.*s^2\sum_{h}V_{hk}\delta\left(u-\frac{h}{a},v-\frac{k}{b}\right)\right].A \qquad (7a)$$

where $s^2=(u^2+v^2)/4$.

On back transformation this becomes

$$\{\psi(x,y)\}=\{C+iS\}'-\frac{\varepsilon\lambda}{4\pi}\sigma\{(C+iS)\nabla^2\varphi_p(x,y)\}', \qquad (7b)$$

where the $\{\}'$ denote Fourier summation over only those coefficients allowed through the aperture.

For an aperture of sufficiently large radius we can use the approximation

$$[Q_{hk}*s^2V_{hk}]\,.\,A\simeq[Q_{hk}\,.\,A]*[s^2V_{hk}\,.\,A],$$

which in real space is equivalent to

$$\{(C+iS)\,.\,\nabla^2\varphi_p(x,y)\}*A\simeq\{C*A+iS*A\}$$
$$\times\{\nabla^2\varphi_p(x,y)*A\}.$$

Thus on back transformation we obtain the intensity distribution to first order in σ and ε,

$$I(x,y)=[\{C^2\}'+\{S^2\}']\left[1-\frac{\varepsilon\lambda}{2\pi}\sigma\{\nabla^2\varphi_p(x,y)\}'\right]. \qquad (8)$$

The first term in equation (8), $\{C^2\}'+\{S^2\}'$, is the contrast observed at the Gaussian focus arising from the intensity scattered outside the lens aperture. The second term is similar to the infinite-aperture expression except that the projected charge density now arises from a truncated summation.

If the intensity distribution at the Gaussian focus is nearly uniform, then equation (8) becomes

$$I(x,y)=1-\frac{\varepsilon\lambda}{2\pi}\sigma\{\nabla^2\varphi_p(x,y)\}',$$

which is almost the same as the infinite-aperture expression [equation (5)] and can be readily computed.

If the contrast at zero defect of focus is too great, for example, because the crystal is too thick or the aperture is too small, then there are still two devices which would allow intuitive interpretation; the better is to divide the image contrast obtained at negative defect of focus [equation (8)] by the contrast obtained at the Gaussian focus $\{C^2\}'+\{S^2\}'$. This should result in quite a good representation of the projected charge density, although division implies some means of picture scanning and processing. The other approximation relies upon the fact that the peaks in the intensity distribution of $\{C^2\}'+\{S^2\}'$ occur in the same position as those for the charge-density distribution. Thus the picture can be interpreted as projected charge density but the peak heights will be in error. This second approximation is obviously less quantitative than the first. It can be improved by subtracting the contrast at zero defect of focus before interpretation and has the advantage that this subtraction process can be done photographically.

It should be noted that if $\{C^2\}'+\{S^2\}'$ is not negligible then it will destroy the antisymmetry about the Gaussian focus and the image will only appear to be like the object for negative defect of focus.

2.4 *Thick crystals*

By using the divided difference form of the analytic solution to the N-beam scattering problem (Moodie, 1972) it can be shown that the scattered wave function $\psi(H)$, within a small range of angles about the origin, can be approximated by the high-voltage-limit form. The range of scattering angles for which the approximation is valid becomes smaller as the crystal thickness is increased. Thus within this small angular range the restricted-aperture charge-density approximation for calculating image contrast will be valid. This approximation is useful for resolutions worse than 20 Å, *i.e.*, values of $(\sin\theta)/\lambda$ less than 0·25 nm^{-1} (Fig. 2).

It can also be used in the interpretation, at high resolution, of the contrast of thin non-periodic features on the surfaces of thick crystals. This application is treated in another publication (Lynch, Moodie & O'Keefe, 1974) and is only briefly mentioned here for the sake of completeness.

2.5 *Lens aberrations*

In a real electron microscope there are three other important parameters which can affect image contrast: astigmatism, chromatic aberration and spherical aberration. In most modern instruments, astigmatism can be corrected to such a high degree of precision that it may be ignored in the interpretation of most images. Chromatic aberration is present to a small extent but its effects are well represented by the addition of intensity of images for a range of defect of focus. This depth of field must be determined for a particular machine.

Resolution (Å)	0	1	5	30	50	100
100	Scherzer	Charge density	Charge density	Charge density	Charge density with absorption	
50	Scherzer	Charge density	Charge density	Charge density	Charge density with absorption	
20	Scherzer	Charge density	N-beam (Charge density for systematics)	N-beam	N-beam with absorption	
5	Scherzer	Charge density	N-beam (Charge density for systematics)	N-beam with absorption	N-beam with absorption	
3·5	Charge density	N-beam	N-beam with absorption	N-beam with absorption	N-beam with absorption	
1·0						

Crystal thickness, H(nm)

Fig. 2. The table shows the simplest imaging calculation applicable for increasing crystal thickness and resolution for incident electron energies of approximately 100 keV ($\lambda=0{\cdot}004$ nm) and atoms of medium atomic weight (as in $Nb_{12}O_{29}$). Scherzer refers to 'the weak-phase-object' approximation; charge density means the 'strong-phase-object' or HVL approximation; while N-beam requires a full N-beam dynamical calculation followed by n-beam imaging of the dynamical complex amplitudes. This figure relates to the scattering process. In a real microscope with finite C_s, reference must be made to Fig. 3 to see whether any particular approximation is physical.

Spherical aberration is of course present in all magnetic lenses and has quite a large effect on the image contrast observed.

If phase changes due to spherical aberration are included in the derivation of the image contrast to first order in ε and σ, the expression becomes

$$I(x,y)=1-\frac{\varepsilon\lambda\sigma}{2\pi}\nabla^2\varphi_p(x,y)+\frac{C_s\lambda^3}{16\pi^3}\sigma\nabla^4\varphi_p(x,y)\,, \quad (9)$$

where C_s is the spherical aberration coefficient. Thus

$$I(x,y)=1-\frac{\lambda\sigma}{2\pi}R(x,y)\,,$$

where

$$R(x,y)=-16\pi^2H\sum_{h,k}\{\varepsilon+2s_{hk}^2\lambda^2C_s\}s_{hk}^2V_{hk} \times\exp\left(2\pi i\left[\frac{hx}{a}+\frac{ky}{b}\right]\right) \quad (10)$$

with $s^2=(\sin\theta)^2/\lambda^2=(u^2+v^2)/4$.

Similar expressions apply for restricted aperture; the $\nabla^2\varphi_p(x,y)$ in equation (8) is replaced by the R in equation (10), the summations now being over those coefficients included in the aperture.

Thus we have the hierarchy of approximations [for instance, in the non-aberrated case, equations (7*b*), (8) and (5)], which, providing certain experimental criteria can be met, permit direct interpretation of image intensity in terms of the object structure, without recourse to the exacting procedures of *N*-beam dynamic calculations.

Fig. 2 shows the appropriate calculation for obtaining agreement with experimental images, at a 10% level of accuracy, as a function of specimen thickness and required image resolution. This figure is drawn for the case of 100 keV electrons and spherical aberration coefficients of the order of 3 mm or better.

The region where naive interpretation is possible is confined to thin crystals at low resolution. For thick crystals at high resolution the complete calculation is in general necessary. Some examples of this latter case can be found in part IV of this series (O'Keefe, 1973), but as yet these calculations have not been compared with experimental images. However, they are believed to be accurate since quite good agreement has been obtained with experimental diffraction intensities in the case of other oxides (Dowell, Goodman & Wilson, 1974).

2.6 *Role of the propagation function*

As shown in equation (4), the validity of the derivation of the hierarchy of approximations depends on the applicability of the expansion of the propagation function.

In the most general case of an apertured lens with spherical aberration, it is necessary to re-examine this expansion. As in Paper IV, the aberrated propagation function is found by substituting $\varepsilon+\frac{1}{2}C_s\lambda^2(u^2+v^2)$ for ε in the non-aberrated form. Thus the aberrated propagator is $\exp\{-i\pi\lambda(u^2+v^2)[\varepsilon+\frac{1}{2}C_s\lambda^2(u^2+v^2)]\}$ and it may be expanded as

$$1-i\pi\lambda(u^2+v^2)[\varepsilon+\tfrac{1}{2}C_s\lambda^2(u^2+v^2)]\,, \quad (11)$$

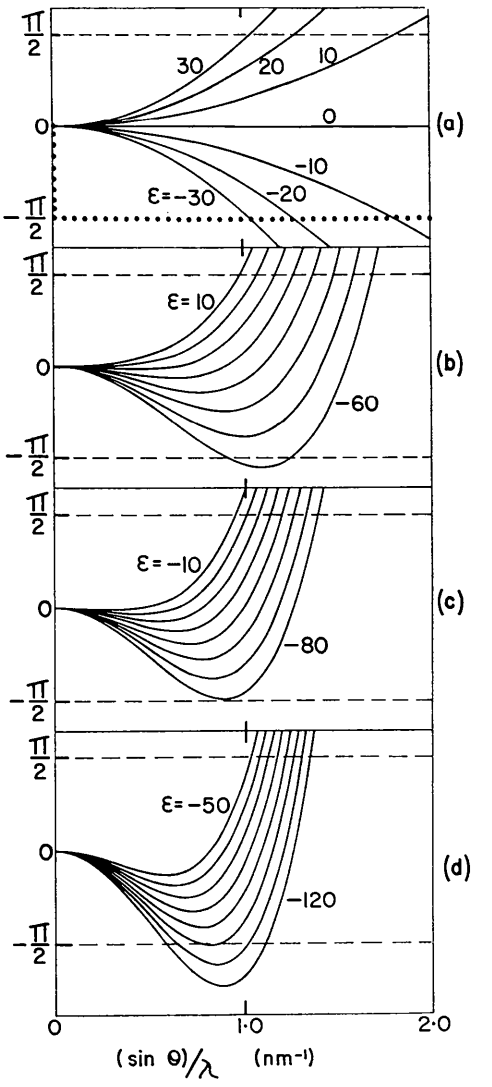

Fig. 3. The propagator argument of equation (11) plotted against s [where $s=(\sin\theta)/\lambda$ and $(2s)^2=(u^2+v^2)$] for spherical aberration coefficients of 0 (*a*), 0·9 mm (*b*), 1·8 mm (*c*) and 2·7 mm (*d*) and an incident electron energy of 100 keV ($\lambda=$ 0·004 nm). Values of the defocus parameter ε (nm) are shown. The dotted line in (*a*) is the idealized propagator required by the weak-phase-object approximation of Scherzer. The PCD approximation requires a parabolic phase change with s with a limit of $-\pi/2$. Thus for $C_s=0{\cdot}9$ mm and $\varepsilon=-60$ nm the requirement is met for resolutions of ≥ 6 Å ($s=0{\cdot}8$ nm^{-1}), while for $C_s=2{\cdot}7$ mm and $\varepsilon=-110$ nm the limit is 8 Å ($s=0{\cdot}6$ nm^{-1}). So long as the propagator remains within the limits $\pm\pi/2$ an aberrated PCD approximation will apply (*e.g.*, for $C_s=0{\cdot}9$ mm and $\varepsilon=-50$ nm this approximation will hold down to resolutions of 3 Å [$s=1{\cdot}6$ nm^{-1})].

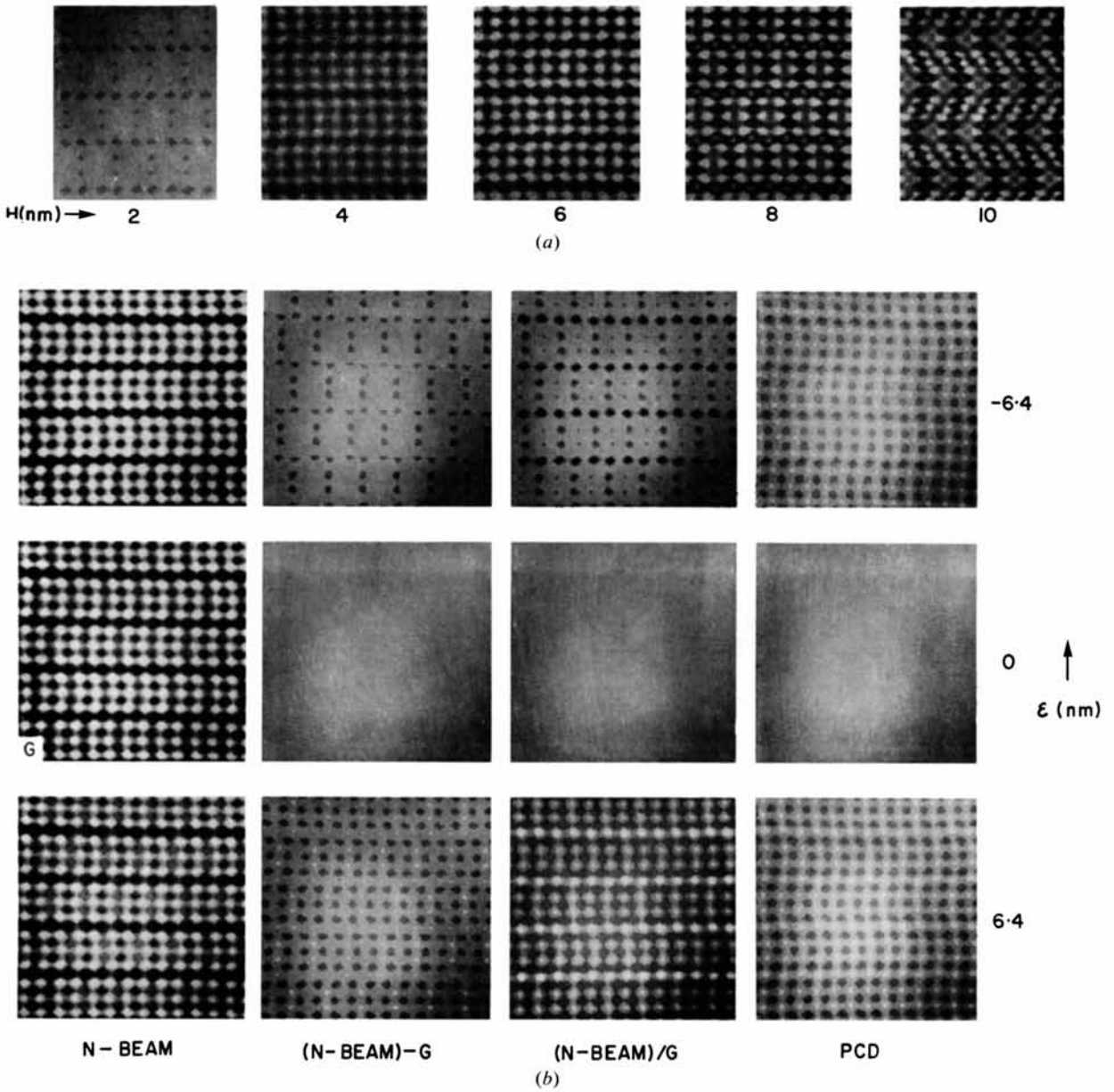

Fig. 4. (*a*) $Nb_{12}O_{29}$ image contrast for zero defocus ($\varepsilon=0$) and zero spherical aberration ($C_s=0$) represents the contrast due to exclusion of beams by the objective aperture. Crystal thickness, H, ranges from 2 nm to 10 nm. The aperture was set to allow 39 beams to contribute to the image. Up to 6 nm the zero-defocus N-beam image has peaks in the positions of peaks in the equivalent PCD image. (*b*) Images for −6·4 nm under-focus (top), zero defocus (centre) and 6·4 nm over-focus (bottom) for a 5 nm thick crystal of $Nb_{12}O_{29}$. The aperture was set to allow 39 beams to contribute to the images. The N-beam image (column 1) is dominated, at both under- and over-focus, by the zero-defocus contribution (G). when the zero-defocus contrast is subtracted (column 2) or divided out (column 3) the complementarity of under- and over-focus images which exists in the PCD images (column 4) is to some extent restored.

[*To face p.* 304

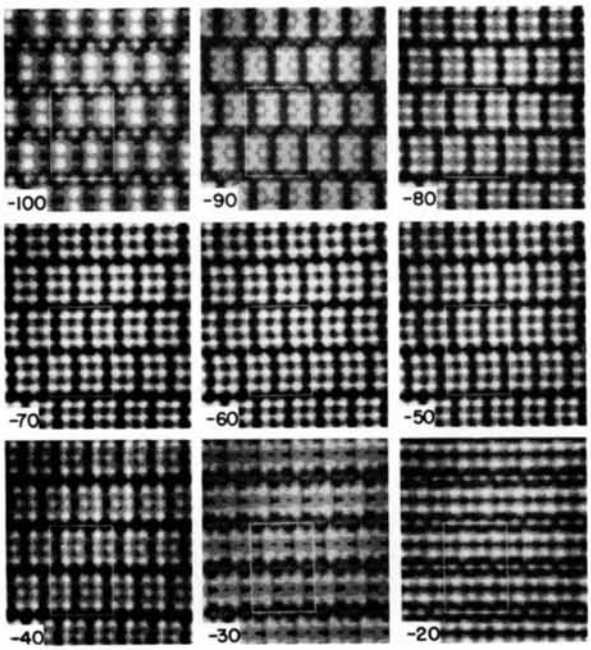

(a)

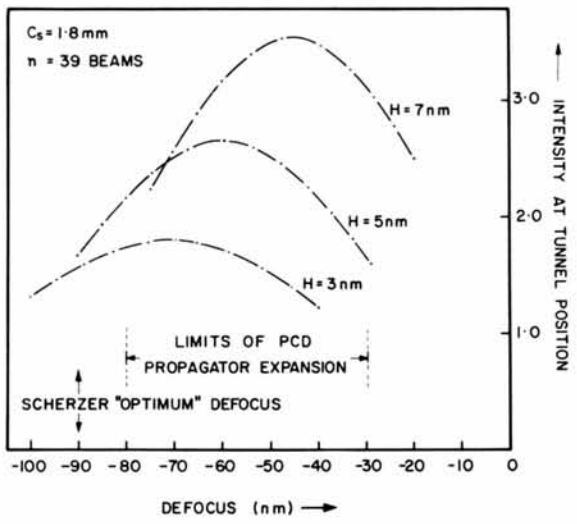

(b)

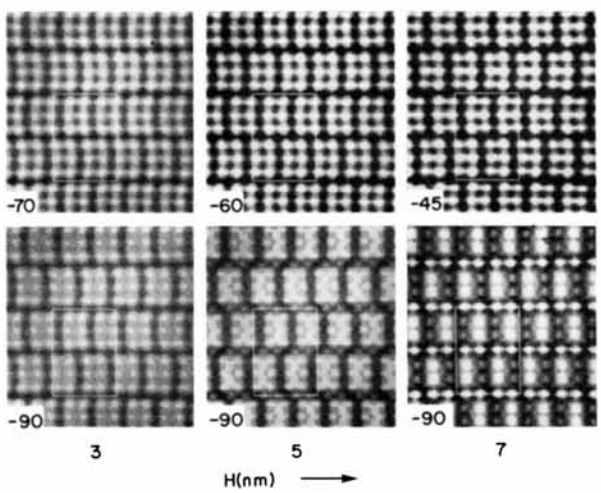

(c)

Fig. 5. (*a*) *N*-beam lattice images of $Nb_{12}O_{29}$ calculated for $n=39$, $C_s=1{\cdot}8$ mm, $H=5$ nm and defects of focus from -100 to -20 nm in 10 nm steps. As the defect of focus approaches the value yielding the best image ($\varepsilon=-60$ nm), the character of the image becomes stationary with respect to defocus. As the value of ε becomes further away from the best value then image character changes rapidly. (*b*) Maximum contrast in *N*-beam lattice images plotted as a function of defocus for crystals of $Nb_{12}O_{29}$ of three thicknesses. Spherical aberration is $C_s=1{\cdot}8$ mm and $n=39$. The graphs cover only that range of defocus where the maximum image intensity occurs at tunnel sites. For each thickness the 'best' or intuitively interpretable image occurs at the maximum of the curve. (*c*) *N*-beam lattice images of $Nb_{12}O_{29}$ calculated for $n=39$, $C_s=1{\cdot}8$ mm and crystals of thickness $H=3$, 5 and 7 nm. The top row of images is calculated for the defects of focus yielding maximum intensity at tunnel sites. The lower row of images is calculated for the Scherzer 'optimum' defocus of -90 nm. For the two thicker crystals the image obtained at the Scherzer condition does not look like the structure.

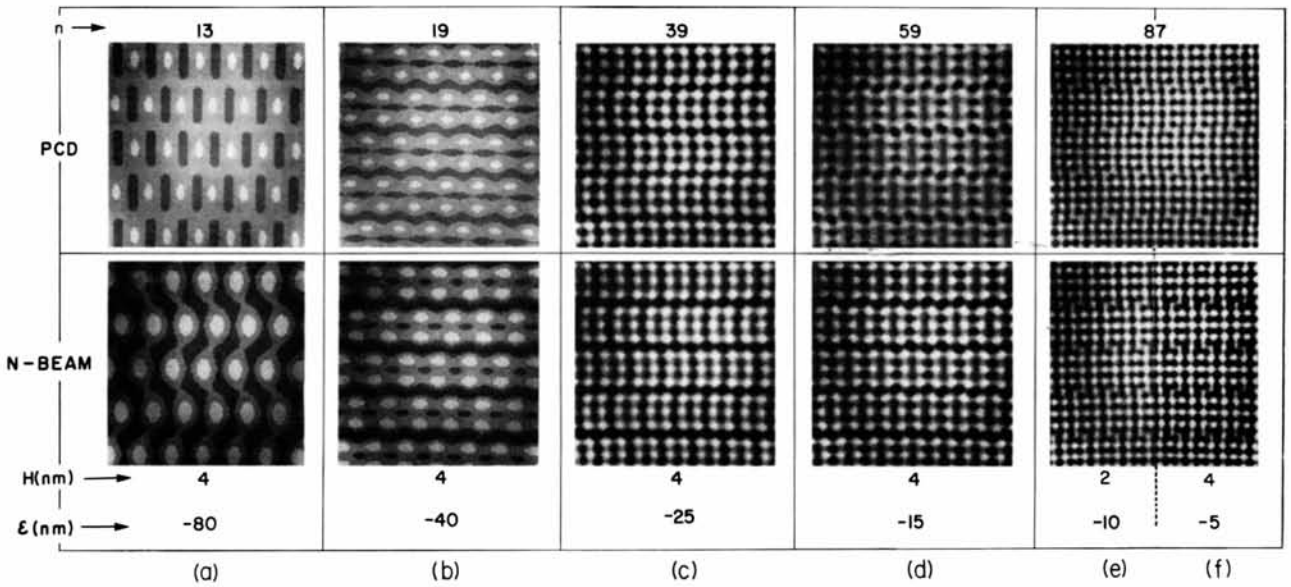

Fig. 6. PCD images (top) compared with N-beam images (bottom) for increasing aperture (better resolution) and crystal thickness $H=4$ nm. Spherical aberration is zero and ε is kept such that $\pi\varepsilon\lambda(u^2+v^2)<\pi/2$ and $\varepsilon H\sigma\lambda/2\pi\nabla^2\varphi_p^*(x,y)<1$. For low numbers of beams the PCD approximation breaks down [*e.g.*, (*a*) $n=13$], but as n increases the fit becomes better [*e.g.*, (*b*) $n=19$, (*c*) $n=39$ and (*d*) $n=59$]. At better resolutions crystal thickness becomes more critical (Fig. 2) so that at $H=4$ nm the N-beam contrast is greater than that of the PCD image [*e.g.*, (*d*) $n=59$ and (*f*) $n=87$]; when H is lowered to 2 nm (εH being kept constant) the fit for large n improves [*e.g.*, (*e*) $n=87$, $H=2$ nm is closer to the n-PCD image than (*f*) $n=87$, $H=4$ nm].

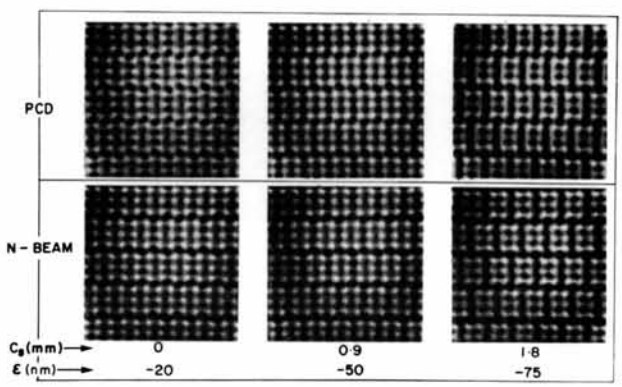

Fig. 7. Aberrated PCD images show good agreement with aberrated N-beam images for crystals of thickness $H=3$ nm and spherical aberration coefficients of (*a*) 0, (*b*) 0·9 mm and (*c*) 1·8 mm. The defocus ε (marked) is chosen so that the aberrated-propagator argument remains within $\pm\pi/2$.

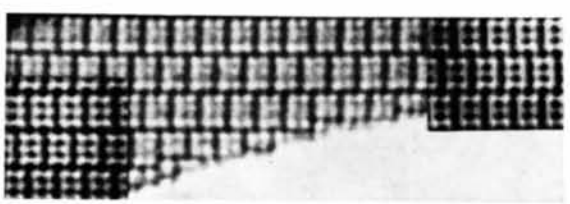

Fig. 8. Experimental image of $Nb_{12}O_{29}$ (courtesy S. Iijima). Inserts: left-hand side shows the N-beam image calculated for $n=59$, $C_s=1{\cdot}8$ mm, $H=3$ nm and $\varepsilon=-75$ nm; right-hand side shows the PCD image calculated for the same values of the parameters n, C_c, H and ε.

if the argument (second term) is less than one within the aperture.

In Fig. 3 the argument in the propagation function is shown as a function of scattering angle for a variety of defects of focus and spherical aberration coefficients. Fig. 3 also shows the argument that is required in the Scherzer (1949) approach, *i.e.* zero at the origin and $-\pi/2$ elsewhere within the aperture. As can be seen, when the spherical aberration is zero, the argument of equation (11) has a parabolic form [equation (4)] and is symmetrical about zero defect of focus. This is the form of the argument which leads to a direct interpretation in terms of the restricted-aperture projected charge density for negative defect of focus. For larger apertures the range of validity as a function of defect of focus becomes smaller. Of course, there is also a definite lower limit to the aperture size, which is dependent on the structure. As the spherical aberration coefficient is increased in magnitude the aperture size for which the argument of the propagation function is nearly parabolic becomes smaller. However, for smaller ranges of defect of focus, the argument remains within the bounds of $\pm\frac{1}{2}\pi$ and thus the image can be interpreted as the projected charge density viewed through a spherically aberrated lens. Finally, with further increase in the spherical aberration coefficient, the excursions in the argument of the propagation function are so large that the approximation is only valid for low-resolution work (greater than 20 Å).

It is of interest to note in Fig. 3 that the comparison of the Scherzer curve with a curve typical of a modern microscope illustrates that the Scherzer-type approximation to the propagation function is quite inaccurate.

3. Experimental criteria

Our object is to compare images calculated by the precise methods used in part IV with those calculated by the various approximations described above, in order to illustrate the bounds of validity of these approximations, and finally to demonstrate agreement with experimental images. The substances chosen as examples are mixed titanium–niobium oxides, because of the many good images of these materials which have appeared in the literature (Iijima, 1971; Allpress & Sanders, 1973). The results show the conditions for validity of the charge-density approximation. The computed images were obtained as half-tone displays on a storage oscilloscope (Billington & Kay, 1974).

3.1 *Crystal thickness*

Fig. 4(*a*) illustrates the effect of specimen thickness on the image. As the specimen becomes thicker more of the energy is scattered outside the aperture and thus the amount of image contrast in the apertured zero-defect-of-focus image becomes more appreciable. It can be seen that the contrast at zero defect of focus for a crystal of 6 nm thickness has peaks in the same place as the projected structure and so a naive interpretation of the image contrast is still possible provided that the weights of the peaks are not taken into consideration. Fig. 4(*b*) illustrates the effect of the zero defect-of-focus contrast, the $\{C^2\}'+\{S^2\}'$ term of equation (8), on the *N*-beam image, and the degree to which this term may be compensated for in order to obtain a more exact fit with the charge-density approximation. These sets of calculations have been carried out for a spherical aberration coefficient of zero and they have application only to low-resolution images obtained from a real electron microscope. Thus we see that, for a zone-axis orientation of a crystal composed of atoms of medium atomic weight and an accelerating voltage of 100 kV, the crystals should be no thicker than 5 nm. Of course, as the accelerating voltage increases, the crystal thickness can be increased. For a less strongly coupled orientation – for example, a systematics case – the high-voltage limit will hold for a thicker crystal ($\sim$30 nm).

3.2 *Defocus*

3.2.1 *Stationary point*

It is important to note that at the intuitively interpretable defocus (for any particular crystal thickness) the rate of change of image character is at a minimum. This is illustrated for a 5 nm thick crystal of $Nb_{12}O_{29}$ in Fig. 5(*a*). The three central images ($\varepsilon=-70$, -60, -50 nm) differ only slightly, whereas the further the value of ε is from the region of intuitive interpretation, the more rapid is the change of character.

The low rate of change of character with defocus over a range straddling the intuitively interpretable image means that the effects of chromatic aberration (depth of focus) are minimized within this range of defocus.

3.2.2. *Best image*

Within its region of applicability the PCD theory (O'Keefe, 1973) predicts that the value of the defocus parameter of the intuitively-interpretable image approaches zero, as crystal thickness increases. This is easily demonstrated by rewriting equation (5) as

$$I_\varepsilon(x,y)=(C^2+S^2)\left[1-\varepsilon H\frac{\sigma\lambda}{2\pi}\nabla^2\varphi_p^*(x,y)\right],$$

where H is the crystal thickness and $\nabla^2\varphi_p^*(x,y)$ is the projected charge density per unit crystal thickness. For *N*-beam images of $Nb_{12}O_{29}$ calculated for increasing crystal thickness (3, 5, 7 nm) we find a maximum in the intensities of sites corresponding to tunnels in the structure for increasing defects of focus (-70, -60, -45 nm respectively [Fig. 5(*b*)]. However, if the Scherzer criterion for 'optimum' defocus of a thin crystal is applied to these images ($n=39$ beams and $C_s=1{\cdot}8$ mm), we obtain an 'optimum' defocus value of -90 nm. Fig. 5(*c*) shows *N*-beam images at the Scherzer optimum ($\varepsilon=-90$ nm) and at $\varepsilon=-70$, -60 and -45 nm for the three crystal thicknesses.

Examination of the dependence of *n*-beam lattice-image character on defocus shows that the image

which 'looks most like the structure' occurs for the special case of this compound at this aperture, at the defocus where image contrast is a maximum; *i.e.*, where the image intensity at the positions of tunnels in the structure reaches a maximum [Fig. 5(*b*)].

3.2.3 *Propagator*

With $n=39$ for $Nb_{12}O_{29}$ we find $s=(\sin\theta)/\lambda$ has a maximum value of 1·1 nm^{-1}. For this value of s and $C_s=1{\cdot}8$ mm, Fig. 3(*c*) shows that defocus must be within -80 to -30 nm if an interpretation in terms of an aberrated PCD image is to be permitted. Thus, for $H=5$ nm, the images of Fig. 5(*a*) at $\varepsilon=-100$, -90 and -20 nm do not show the charge density and the image at $\varepsilon=-30$ nm is strongly aberrated.

3.3 *Aperture*

The diameter of the aperture must be balanced between the competing requirements of the charge-density approximation and spherical aberration. For easy interpretation the charge-density approximation requires the aperture to be large, while the effect of spherical aberration becomes increasingly strong as the aperture is increased. As the diameter is increased beyond a certain size it can be shown that the spherical aberration coupled with the divergence in the illumination will impose a virtual aperture which can be smaller than the physical aperture, and further increase of the physical aperture will not increase the resolution (O'Keefe & Sanders, 1975).

Fig. 6 illustrates the effect of changing the aperture for a fixed crystal thickness. It can be seen that, for this particular crystal structure, an aperture which includes only 13 beams no longer permits interpretation of the image contrast as the projected charge density of the object. However, once the aperture has been increased to include 39 beams, the agreement is quite good and, in the absence of spherical aberration, the agreement becomes better the larger the aperture. Of course, the permitted range of the defect of focus is much less with a larger aperture. Now, in a real microscope depth of field is determined by chromatic aberration; thus chromatic aberration would start to destroy image contrast at a resolution of the order of 3 Å.

3.4 *Spherical aberration*

Fig. 7 shows the PCD image contrast at a fixed aperture as a function of spherical aberration coefficient compared with the *N*-beam image contrast. At the aperture chosen, once C_s exceeds 2 mm, there is no defect of focus for which the expansion of the propagation function is valid, and a smaller aperture would need to be chosen for such a machine. As can be seen, quite good agreement can be achieved.

4. Comparison with experiment

Finally, Fig. 8 shows the calculation of the projected charge-density approximation, for $Nb_{12}O_{29}$ with an aperture of 59 beams and a spherical aberration coefficient of 1·8 mm, compared with the calculated *N*-beam image and the experimental image obtained by Iijima (private communication). There is quite good agreement. The aperture used in the charge-density calculation is less than the experimental aperture because of the interaction of the spherical aberration of the objective lens with the divergence in the illuminating beam. This effect will be discussed in part VI (O'Keefe & Sanders, 1975) of this series.

5. Conclusions

The above discussion leads us to conclude that naive interpretation of image contrast in terms of the projected charge density of the object is possible provided that:

(*a*) The crystal thickness is sufficiently small that the high-voltage limit for scattering is valid. For 100 keV electrons and elements of moderate atomic number, this puts an effective upper limit on crystal thickness of 5–7 nm in a zone-axis orientation and approximately 30 nm in a systematics orientation (part III).

(*b*) The defect of focus is adjusted on the negative or under-focus side, sufficiently to give adequate contrast but not enough for the propagation-function expansion to become invalid. Again, for current electron microscopes at high resolution, this requirement means a defect of focus of from -50 to -80 nm. The amount of defocus permissible decreases as the aperture size is increased.

(*c*) The aperture is large enough to allow many beams to contribute to the image. This implies of the order of 20 reflexions for a periodic object. The upper limit to aperture size is set in practice by the magnitude of the spherical aberration coefficient and the incident-beam divergence of the machine. In current microscopes this seems to imply a resolution limit at 100 keV of $3\frac{1}{2}$–4 Å (O'Keefe & Sanders, 1975). Thus interpretation of very small features in the image contrast as atoms is quite unreliable unless a proper and complete *N*-beam calculation is carried out. Certainly no naive interpretation of such images is possible.

The above results seem to indicate possible improvements in an electron microscope which would lead to an increase in resolution. One possibility stems from the fact that, if the wavelength is reduced, the high-voltage limit becomes more accurate for thicker crystals. Thus, if an objective lens can be constructed for 200–300 keV electrons with the same spherical aberration coefficient as the current 100 keV lenses, and the quality of the illumination system be improved such that the divergence is 2×10^{-4} rad, then the resolution limit for naive interpretation of a micrograph should become 2 Å at 300 keV–a considerable improvement.

We wish to thank Dr S. Iijima for providing the electron micrograph used in Fig. 8 and permission to

publish it, and Dr J. V. Sanders for comprehensive criticism of the manuscript.

References

ALLPRESS, J. G., HEWAT, E. A., MOODIE, A. F. & SANDERS, J. V. (1972). *Acta Cryst.* A**28**, 528–536.
ALLPRESS, J. G. & SANDERS, J. V. (1973). *J. Appl. Cryst.* **6**, 165–190.
ANSTIS, G. R., LYNCH, D. F., MOODIE, A. F. & O'KEEFE, M. A. (1973). *Acta Cryst.* A**29**, 138–147.
BILLINGTON, C. & KAY, N. R. (1974). *Aust. J. Phys.* **27**, 73–85.
COWLEY, J. M. & MOODIE, A. F. (1960). *Proc. Phys. Soc.* **76**, 378–384.
DOWELL, W. C. T., GOODMAN, P. & WILSON, A. (1974). *Proceedings of International Crystallography Conf., Melbourne*, pp. 308–309.
GOODMAN, P. & MOODIE, A. F. (1974). *Acta Cryst.* A**30**, 280–290.
IIJIMA, S. (1971). *J. Appl. Phys.* **42**, 5891–5893.
LYNCH, D. F. & O'KEEFE, M. A. (1972). *Acta Cryst.* A**28**, 536–548.
LYNCH, D. F., MOODIE, A. F. & O'KEEFE, M. A. (1974). *Proceedings of Eighth International Congress on Electron Microscopy, Canberra*, Vol. 1, pp. 222–223.
MOODIE, A. F. (1972). *Z. Naturforsch.* **27**a, 437–440.
MOODIE, A. F. (1975). To be published.
O'KEEFE, M. A. (1973). *Acta Cryst.* A**29**, 389–401.
O'KEEFE, M. A. & SANDERS, J. V. (1975). *Acta Cryst.* A**31**, 307–310.
SCHERZER, O. (1949). *J. Appl. Phys.* **20**, 20–29.

Acta Cryst. (1975). A**31**, 307

n-Beam Lattice Images. VI. Degradation of Image Resolution by a Combination of Incident-Beam Divergence and Spherical Aberration

BY M. A. O'KEEFE AND J. V. SANDERS

CSIRO Division of Tribophysics, University of Melbourne, Parkville, Victoria 3052, *Australia*

(*Received* 5 *November* 1974; *accepted* 20 *December* 1974)

Lattice images were computed with increasing incident-beam divergence with spherical aberration taken into account. The effect is as if the outer diffracted beams transmitted by the objective aperture do not contribute to the image, so that the resolution is effectively less than that expected from the aperture size. Images of $Nb_{12}O_{29}$, calculated with the inclusion of this effect, show improved agreement with experimental images.

1. Introduction

An electron microscope without aberrations would give a lattice image of great detail and contrast, which could be simply interpreted if the specimen were thin enough. The most important aberration is, of course, spherical aberration of the objective lens, and its effect on the image is generally reduced by inserting an objective aperture to exclude the diffracted beams whose phases are most severely modified. The aperture size is usually carefully selected to match the value of the spherical aberration coefficient (C_S) of the objective lens (Scherzer, 1949). The effects of spherical aberration and of the introduction of an objective aperture introduce complications into the interpretation of the lattice image, and these have been discussed in general in part I,* in Allpress & Sanders (1973) and in detail in part IV.* It was shown in part IV that for a thin-enough crystal, the image could be simply approximated by calculating a 'restricted, projected charge density' (*n*-PCD) image, which had a resolution determined by the number of diffracted beams, *n*, which were transmitted through the objective aperture.

Earlier in this series, the other aberrations introduced into the lattice image by the imperfections in the electron microscope were classified into two groups:

(*a*) those which modify the image, but without loss of detail; and

(*b*) 'smearing' aberrations which produce overlapping differences in detail and hence result in loss of detail; for example the energy spread of the electrons produces an indefiniteness into the position of the image plane, and hence produces the superposition of a number of different images in any selected image plane.

A consideration of the effect of these various aberrations showed that, of those of the 'smearing' type, the divergence of the incident illumination could be the most important. Two ways in which divergence influenced the image were previously considered:

(i) The amplitudes and phases of the diffracted beams depend upon the angle of incidence of the electron beam. For crystals thin enough to satisfy *n*-PCD

* Previous papers in this series are: Part I – Allpress, Hewat, Moodie & Sanders (1972). Part II – Lynch & O'Keefe (1972). Part III – Anstis, Lynch, Moodie & O'Keefe (1973). Part IV – O'Keefe (1973). Part V – Lynch, Moodie & O'Keefe (1975).